Thin-Walled Structures 48 (2010) 905–914

Contents lists available at ScienceDirect

Thin-Walled Structures

journal homepage: www.elsevier.com/locate/tws

Strengthening of perforated plates under uniaxial compression: Buckling analysis

Bin Cheng *, Jincheng Zhao

Department of Civil Engineering, Shanghai Jiao Tong University, Room A508, Ruth Mulan Chu Chao Building, No. 800 Dong Chuan Road, Shanghai 200240, China

ARTICLE INFO

Article history:
Received 25 April 2010
Received in revised form
24 May 2010
Accepted 2 June 2010
Available online 1 July 2010

Keywords:
Perforated plate
Circular hole
Uniaxial compression
Elastic buckling stress
Elasto-plastic ultimate strength
Cutout-strengthening

ABSTRACT

This paper focuses on the cutout-strengthening of perforated steel plates subjected to uniaxial compressive loads. The square plates considered each has a centrally placed circular hole and four simply supported edges in the out-of-plane direction. Four types of stiffeners named ringed stiffener (*RS*), flat stiffener (*FS*), longitudinal stiffener (*LS*) and transverse stiffener (*TS*) are mainly discussed. The finite element method (FEM) has been employed to analyse the elastic and elasto-plastic buckling behaviors of strengthened and unstrengthened perforated plates. The results show that the strengthened perforated plates have higher buckling strengths than those of the unstrengthened ones, while the elevations in elastic buckling stress and elasto-plastic ultimate strength are closely related to stiffener types (i.e., *RS*, *FS*, *LS* and *TS*) as well as plate geometric parameters (i.e., a plate slenderness ratio and a hole diameter ratio). Furthermore, comparisons of strengthening efficiency considering the variations of buckling stress with stiffener weight are carried out, and recommendations on the most efficient cutout-strengthening methods for the uniaxially compressed perforated square plates with centric circular holes are proposed.

1. Introduction

Cutouts are often provided in plate structures such as cold formed steel members, plate and box girders, box pylons and ship grillages for the purposes of access, services and even aesthetics. The presence of holes in such structures results in a redistribution of the membrane stresses accompanied by a change in mechanical behaviors of the plates. Concretely, a significant reduction in elasto-plastic ultimate strength, when compared to solid plate (i.e., imperforated plate), has always been found in perforated plates notwithstanding the occasionally occurring increase in elastic buckling critical load as reported in previous articles. When the cutout is inevitable for the plates under high working stress, the reduced buckling strength of the perforated plate may be insufficient to meet the requirements of normal serviceability and structural safety. It is necessary, hence, to adopt an appropriate cutout-strengthening method to improve the buckling behaviors (including elastic buckling critical stress and elasto-plastic buckling ultimate strength) of perforated plates in these situations.

A large number of researches have been undertaken on the buckling behavior of perforated plates and the main concerns in published articles can be classified into two categories, i.e., elastic buckling and elasto-plastic buckling. For elastic buckling, Shanmugam and Narayanan [1] and Sabir and Chow [2] firstly used the finite element method (FEM) to predict the elastic buckling stress of perforated square plates with different loadings and edge conditions. The conjugate load/displacement method (CLDM) was then successfully applied by Yettram, Brown and Shakerley [3–6] to the elastic buckling analysis of square plates with centric/eccentric rectangular perforations, accompanied by design guidance about geometric size, location and orientation of the rectangular hole. El-Sawy and Nazmy [7] investigated the effect of aspect ratio on the elastic buckling critical loads of uniaxially loaded rectangular plates with eccentric circular and rectangular (with curved corners) holes. El-Sawy and Martini [8] employed the finite element method to determine the elastic buckling stresses of biaxially loaded perforated rectangular plates with longitudinal axis located circular holes. Moen and Schafer [9] developed closed-form expressions for approximating the influence of single or multiple holes on the elastic buckling critical stress of plates in bending or compression. As for elasto-plastic buckling, Narayanan and Rockey [10] described the ultimate strength tests on thin-walled webs containing a circular hole and presented a method to approximately predict the ultimate capacity of plate girders with perforated webs. Azizian and Roberts [11] carried out the geometrically nonlinear elasto-plastic analysis using finite element method for axially compressed square plates with centrally placed square and circular holes. Narayanan and Chow [12] presented an approximate method of

* Corresponding author. Tel./fax: +86 21 34207985.
E-mail address: cheng_bin@sjtu.edu.cn (B. Cheng).

0263-8231/$ - see front matter © 2010 Elsevier Ltd. All rights reserved.
doi:10.1016/j.tws.2010.06.001

predicting the ultimate load carrying capacity of simply supported perforated plates under uniaxial compression, whose reliability was validated by comparing with test results. Curves suitable for the use of designers have also been proposed in the paper to determine the ultimate capacity of square plates with centrally placed holes. Shanmugam et al. [13] proposed a design formula, on the basis of the results from the finite element analyses, to determine the ultimate load carrying capacity of perforated square plates with square or circular holes for the cases of different boundary conditions and uniaxial or biaxial compression. El-Sawy et al. [14] focused on the elasto-plastic buckling of uniaxially loaded square and rectangular plates with circular cutouts by the use of the finite element method, including some recommendations about hole size and location for the perforated plates of different aspect ratios and slenderness ratios. Paik [15–17] investigated the ultimate strength characteristics of perforated plates under edge shear loading, axial compressive loading and the combined biaxial compression and edge shear loads, and proposed closed-form empirical formulae for predicting the ultimate strength of perforated plates based on the regression analysis of the nonlinear finite element analyses results. Maiorana et al. [18,19] dedicated to the linear and nonlinear finite element analyses of perforated plates subjected to localized symmetrical load. In summary, the elastic and elasto-plastic buckling behaviors of perforated plates with different aspect ratios (square and rectangular), slenderness ratios, hole shapes (square, circular, rectangular and rectangular with curved corners) and hole locations (centric and eccentric) have been systematically studied in previous researches, and conclusions, suggestions and formulations beneficial for practical engineering design have also been presented. However, most of them focused on the changes in buckling behavior of perforated plates due to the presence of cutouts. The cutout-strengthening methods used for improving the degraded buckling behavior of perforated plates have not been investigated in published literatures.

Herein, this paper is dedicated to the bucking analyses of strengthened perforated steel plates under uniaxial compression. The studied square plates with centric circular holes are considered to be simply supported on all edges. Four types of stiffeners, i.e., ringed stiffener, flat stiffener, longitudinal stiffener and transverse stiffener, are taken into account. A series of profound investigations of both elastic and elasto-plastic buckling behaviors for strengthened and unstrengthened perforated plates are carried out by the use of the ANSYS finite element method, since the elastic buckling stress and elasto-plastic ultimate strength are useful for the serviceability limit state (SLS) and ultimate limit state (ULS) design purposes, respectively. In addition, recommendations on the most efficient cutout-strengthening methods for the uniaxially compressed perforated square plates with different slenderness ratios and circular hole diameter ratios are proposed on the basis of contrastive analyses of strengthening efficiency considering varying stiffener weights (i.e., stiffener sizes) for each stiffener type.

2. Perforated square plates

2.1. Geometry

The perforated square plates, with a centric circular hole for each one, are employed as research objects in this paper. The following two geometric parameters have been considered:

- plate slenderness ratio b/t, varying from 20 to 100 with increment of 10,
- hole diameter ratio d/b, varying from 0.1 to 0.5 with increment of 0.1,

where b and t are the width and thickness of the square plate, and d is the diameter of the circular hole, as shown in Fig. 1.

Four types of stiffeners named ringed stiffener (*RS*), flat stiffener (*FS*), longitudinal stiffener (*LS*) and transverse stiffener (*TS*) are considered in the present paper due to their wide applications in practical engineering. The details of the strengthened perforated plates are shown in Fig. 2:

(1) For the *RS*-strengthened plate, a strengthening stiffener with thickness of t_a and width of h_a is symmetrically welded to the perforated plate at their circular intersections after being rolled into a ring with outer diameter d.
(2) For the *FS*-strengthened plate, three fabricating steps are normally suggested. Firstly, a circular hole with diameter of $(d+2t_b)$, where t_b is the thickness of square flat stiffener with width of L_b, should be perforated in the center of the stiffener. The perforated stiffener, then, is tightly attached to the surface of the plate strengthened with two circles in the plate and the stiffener being concentric. The welding is finally carried out along the inner (hole) edge and the four outer edges of the flat stiffener.
(3) For the *LS*-strengthened or *TS*-strengthened plate, the two stiffeners with thickness of t_c or t_d and width of h_c or h_d are parallel or perpendicular to the load direction after being welded to the perforated plate, and the smallest distance between hole edge and stiffener's surface, as used for welding, is selected as the same value of stiffener thickness (t_c or t_d).

Considering the common situations of practical engineering, the geometric sizes (interpreted in Fig. 2) of stiffeners selected in the following analyses take the values as follows:

- For ringed stiffener (*RS*), $t_a=0.5t$, $h_a=10t_a$.
- For flat stiffener (*FS*), $t_b=0.5t$, $L_b=1.8d$, $\theta_b=90^\circ$.
- For longitudinal stiffener (*LS*), $t_c=0.5t$, $h_c=8t_c$.
- For transverse stiffener (*TS*), $t_d=0.5t$, $h_d=8t_d$.

Note that there is another layout of flat stiffener where the stiffener's outer edges and plate's edges are skew (e.g., $\theta_b=45^\circ$). But it has been proved by the authors' analyses that the buckling stresses (including elastic and elasto-plastic) of $\theta_b=45^\circ$ are slightly smaller than those of $\theta_b=90^\circ$ (with result differences being no more than 4%). Therefore, this article only considers the case of $\theta_b=90^\circ$.

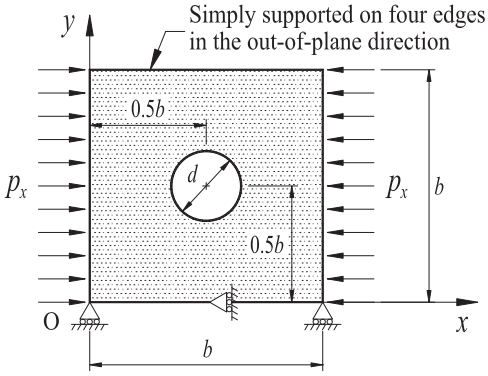

Fig. 1. The unstrengthened square plate with a centrally placed circular hole.

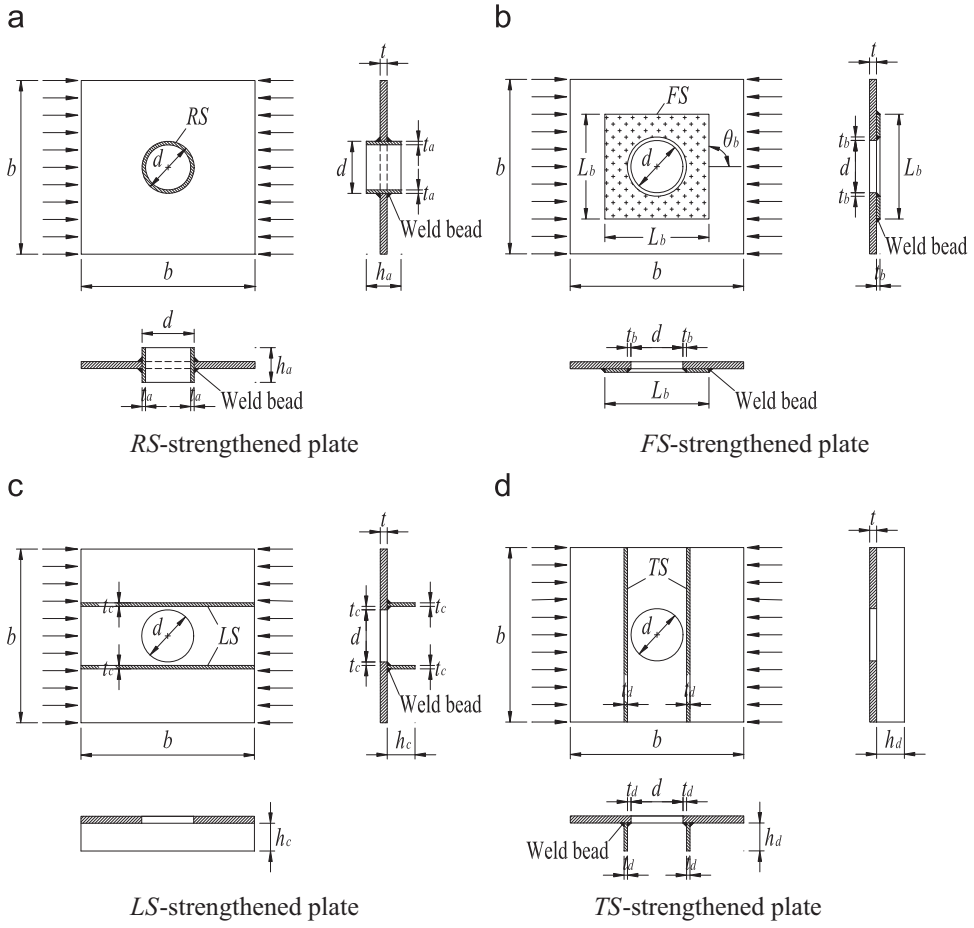

Fig. 2. The strengthened perforated square plate with a centric circular hole.

2.2. Boundary conditions

A perforated plate in practical structure is normally supported by the adjacent plates and thus is in the state between rotatable constraint and fixed constraint in the out-of-plane direction. The studied plates, therefore, are considered to be simply supported on all edges in the present study, as shown in Fig. 1. It means that the lateral deflection stiffnesses on the boundaries are infinite and the rotational stiffnesses on the edges are infinitesimal. It has been proved by previous researches that this approximation always gives slightly conservative results for practical engineering.

Furthermore, some in-plane boundary conditions should be applied to the finite element model considering the nonoccurrence of rigid-body movement and the permission of translational displacement in the plate plane. In this paper, the middle point of the bottom edge is restrained in the x direction (i.e., load direction) and the degrees of freedom of the two bottom corners are fixed in the y direction, as shown in Fig. 1.

2.3. Load case

Since the steel plates are perforated to satisfy the special service functions in most of the occasions, the lateral loads are almost impossible to be applied on the plate surface. Hence, it is appropriate to only take in-plane loads including compression, tension and shear into consideration during the mechanical analysis of perforated plates. In the present study, only longitudinal uniform compression in the x direction is considered, as shown in Fig. 1. Other load cases such as biaxial compression and edge shear loading will be discussed in the authors' subsequent research papers.

3. Analysis method and FE model

3.1. Basic hypotheses

The study is based on the following assumptions:

1. The perforated plate and the stiffener are composed of the same isotropic material.
2. The load effect of steel weight is ignored.
3. The perforated plate and the stiffener are rigidly connected at their intersections.
4. The influences of weld bead size and welding induced residual stress are ignored.

3.2. Buckling analysis method

As we know, the governing equation for the finite element analysis can be written in incremental representation as follows:

$$\Delta R = (K_0 + K_\sigma)\Delta u \tag{1}$$

where K_0 is the constant stiffness matrix related only to the geometric sizes of the plate, K_σ is the current stress stiffness matrix, Δu is the incremental displacement vector and ΔR is the corresponding incremental force vector.

When elastic buckling occurs, the plate has increase in its displacements (i.e., Δu) with no increase in the load or force (i.e., ΔR). It can be concluded from Eq. (1) that $|K_0+K_\sigma|=0$ is satisfied. Taking advantage of the proportional relationship between current stress stiffness matrix (K_σ) and actual stress inside the plate in the case of small deformation, the elastic buckling coefficient (k) can be easily determined by solving a typical eigenvalue equation. The elastic buckling critical stress (σ_{cr}) can be written as

$$\sigma_{cr}=k\frac{\pi E}{12(1-\nu^2)}\left(\frac{t}{b}\right)^2 \tag{2}$$

where E and ν represent Young's modulus and Poisson's ratio of steel, respectively.

While for elasto-plastic buckling analysis, the situation becomes more sophisticated since the current stress stiffness matrix K_σ is no longer proportional to the actual stress in the plate due to the influence of geometric nonlinearity and material nonlinearity. In other words, the essence of elasto-plastic buckling analysis is the solve-seeking process of the equilibrium equations in which both geometric and material nonlinearities were considered. Hence, in order to obtain the elasto-plastic ultimate strength (σ_{xu}) of the perforated plate, a general-purpose finite element program should be used for the whole process analysis of the plate by gradually increasing the loads applied on the plate until collapse occurs. In this paper, the collapse is deemed to happen at the peak point of in-plane load versus out-of-plane deflection relation curve and the elasto-plastic ultimate strength takes the greatest load during the whole loading process. The arc-length method has also been employed for solving the nonlinear equations, in order to avoid the solving instability near the load–deflection curve peak.

3.3. Finite element model

The steel used in this study has the material properties of yield stress $\sigma_y=345$ MPa, Young's modulus $E=2.1\times10^5$ MPa and Poisson's ratio $\nu=0.3$. During elasto-plastic analysis, the steel material is assumed to be linearly elastic before yielding and perfectly plastic after yielding (i.e., with no strain hardening). The initial geometric imperfection follows the elastic buckling mode and the initial deflection amplitude is chosen to be $b/1000$.

Plate elements (SHELL181) with four nodes and six degrees of freedom for each node were used in the present research, with the influence of transverse shear deformation being considered [20]. The meshes around the circular hole and near the stiffeners are subdivided to take into account the complexity of stress distribution inside these zones. The mesh-controlling parameters for analyses are selected as follows:

1. For the unstrengthened plate, the element sizes along the plate edges and the hole edge are $b/30$ and $(\pi d)/120$, respectively, indicating that the element size gradually increases by 12.5–2.5 times (for $d/b=0.1$–0.5) from the hole edge to the plate edges.
2. For the *FS*-strengthened plate:
   - the element size along the plate edges is $b/30$,
   - the element size along the four straight intersections of plate and stiffener is $L_b/30$,
   - the element size along the plate's hole edge and the stiffener's hole edge is $(\pi d)/120$.
3. For the plates strengthened by *RS*, *LS* and *TS*:
   - the element size along the plate edges is $b/30$,
   - the element size along the hole edge is $(\pi d)/120$
   - the average element size in the stiffener is $(\pi d)/120$.

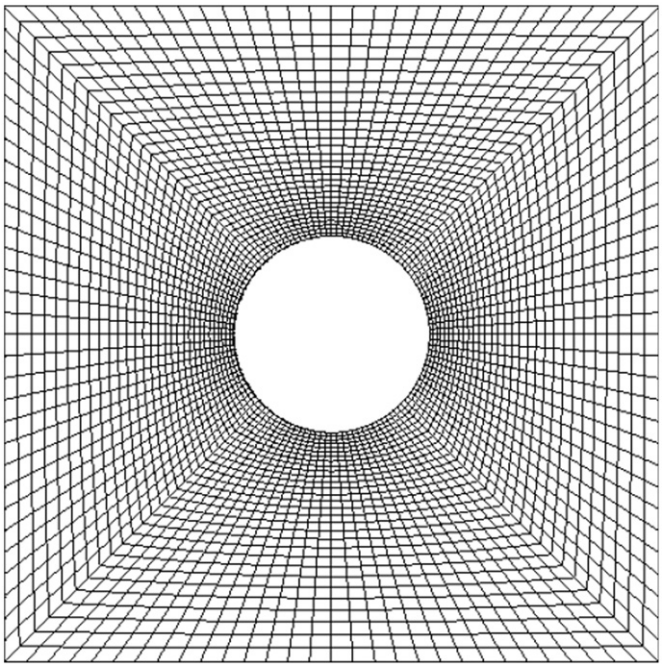

Fig. 3. Finite element meshes of the unstrengthened perforated plate with $d/b=0.3$.

The typical finite element meshes of an unstrengthened perforated plate produced with the previous selected mesh-controlling parameters are demonstrated in Fig. 3. It is noted that, for the *FS*-strengthened plate, the degrees of freedom (DOFs) of the nodes in the outer straight and inner circular edges of the flat stiffener are coupled with those of perforated plate nodes located in the same plane position, while the other nodes in the two elements are separated in the finite element model. The node DOF coupling treatment, as shown in Fig. 4, is regarded by the authors as the best way for simulating the connecting effect of weld beads appearing in practical structures. In the finite element model, the perforated plate and the flat stiffener are located in two parallel planes whose distance equals to $(t+t_b)/2$. Hence, for each weld line, there are two lines, named stiffener line *A* and plate line *B*, whose in-plane coordinates are identical and out-of-plane coordinates are different. For a stiffener node *I* in line *A*, the nearest plate node *J* in line *B* is firstly selected and the DOFs of node *I* are completely coupled with those of node *J*.

To verify the applicability of the selected mesh-controlling parameters, a mesh sensitivity study is carried out for the plates with plate slenderness ratios $b/t=20$ and 100 and hole diameter ratios $d/b=0.1$, 0.2, 0.3, 0.4 and 0.5. The buckling analysis results produced by the selected mesh-controlling parameters are compared to those of half-size refined meshes, which are regarded as most accurate. The results show that the average error and the maximal error of buckling strengths (including elastic buckling stresses and elasto-plastic ultimate strengths) are 0.32% and 0.64%, respectively, which is considered accurate enough for the research.

4. Buckling analysis results

4.1. Elastic buckling behavior

Fig. 5 shows the variations of elastic buckling stress (σ_{cr}) for unstrengthened and strengthened perforated plates with slenderness ratios $b/t=30$ and 90, as plotted against the hole diameter ratio d/b. The following are evident from Fig. 5:

1. Cutout-strengthening produces no weakening in the plate's elastic buckling behavior since σ_{cr} of perforated plates

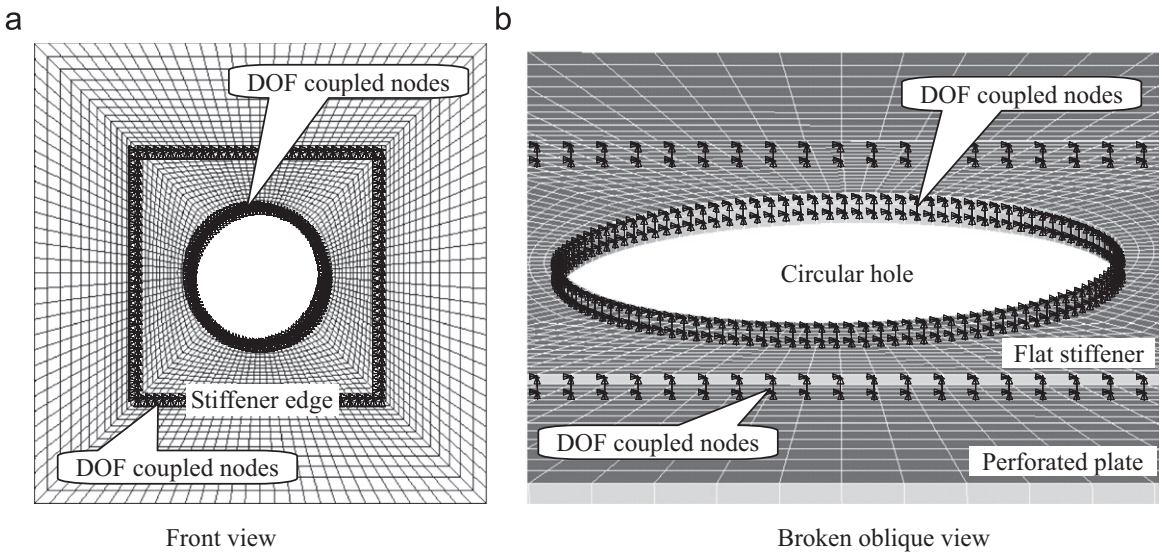

Fig. 4. Node DOF coupling for the *FS*-strengthened perforated plate.

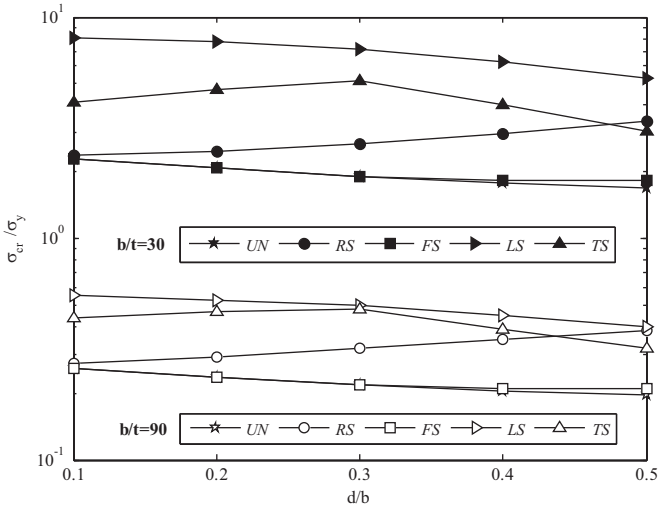

Fig. 5. Elastic buckling stresses of unstrengthened and strengthened perforated plates with $b/t=30$ and 90.

strengthened by the four types of stiffeners are more or less increased when compared to unstrengthened plates. For the cases of $b/t=30$, σ_{cr} of perforated plates strengthened by *RS*, *FS*, *LS* and *TS* are, respectively, 0.04–1.01, 0–0.09, 2.15–2.74 and 0.81–1.71 times higher than those of unstrengthened plates. While for the cases of $b/t=90$, the increases in σ_{cr} of four types of strengthened plates, when compared to unstrengthened plates, are 6–97%, 0–8%, 105–129% and 63–119%, respectively. On the whole, the discussed stiffeners have better strengthening effects for thick plates than for thin plates. Moreover, it can be concluded from comparison of four stiffener types that *LS* brings the greatest enhancement in σ_{cr}, followed by *TS*, and *FS* has almost zero contribution to elastic buckling stress.

2. When d/b remains constant, σ_{cr} of all strengthened perforated plates fall rapidly with increase in b/t, which is similar to unstrengthened perforated plates and imperforated plates.
3. The influence of hole diameter ratio on elastic buckling stress has no relation to plate slenderness ratio, but is not exactly the same for different stiffener types. Concretely, σ_{cr} of *FS*-strengthened and *LS*-strengthened plates decrease simultaneously with increase in d/b and the reverse is true for *RS*-strengthened plates. While for the *TS*-strengthened plates, there lies a peak point near $d/b=0.3$ in each σ_{cr} curve (i.e., σ_{cr} first increases as d/b is enlarged from 0.1 to 0.3 and then decreases as d/b is enlarged from 0.3 to 0.5), even for all considered plate slenderness ratios ($b/t=20$–100).

Further studies on elastic buckling mode have been carried out and the typical buckling shapes of unstrengthened and strengthened perforated plates with plate slenderness ratio $b/t=90$ are demonstrated in Fig. 6. It is clear that the strengthened perforated plates, in addition to the *TS*-strengthened plates with small holes, show the same buckling characteristics (i.e., one half wave in both the x and y directions) with the unstrengthened perforate plates. It can be concluded that the increases in σ_{cr} of strengthened perforated plates, as shown in Fig. 5, are derived from the enhanced out-of-plane stiffnesses provided by the ringed or lateral placed stiffeners. But for the *TS*-strengthened plates with small holes (e.g., $d/b=0.1$), the buckling mode is quite different from others and has two half waves in the x direction. In these cases, the out-of-plane stiffness of the plate becomes larger with increase in d/b, since the transverse stiffeners are closer to the mid-span of buckling half wave as the hole size is increased. When the centrally placed hole is enlarged to a critical value, the transverse stiffeners are farther away from the mid-span of buckling half wave as d/b is increased, due to the transformation of buckling mode from two half waves into single half wave (in the x direction). This may be a plausible explanation for the phenomenon of peak points in *TS* curves as shown in Fig. 5.

4.2. Elasto-plastic buckling behavior

Variations of elasto-plastic ultimate strength (σ_{xu}) of unstrengthened and strengthened perforated plates with slenderness ratios $b/t=30$ and 90 are demonstrated in Fig. 7, as plotted against the hole diameter ratio d/b. The following are found:

1. Similar to elastic buckling stresses, σ_{xu} of all perforated plates discussed in this paper are enhanced by each type of stiffener. For the cases of $b/t=30$, the increases in σ_{xu} of perforated plates strengthened by *RS*, *FS*, *LS* and *TS*, when compared to unstrengthened plates, are, respectively, 7–43%, 4–42%, 5–21% and 2–10%, with high values occurring for large hole diameter

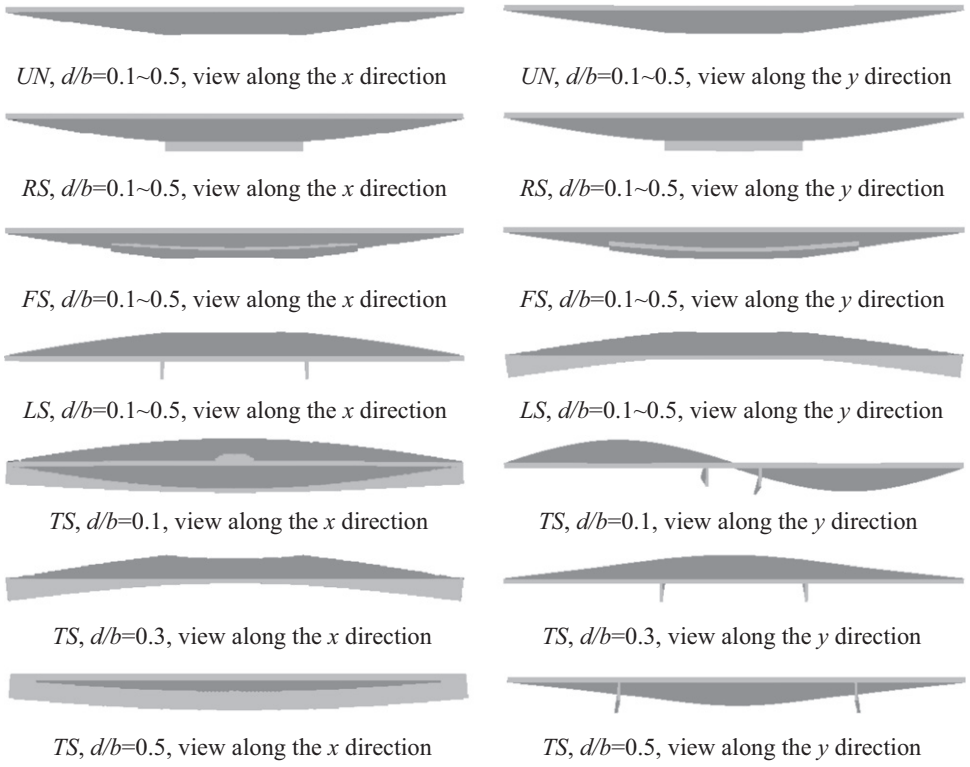

Fig. 6. Elastic buckling modes of unstrengthened and strengthened perforated plates with $b/t=90$.

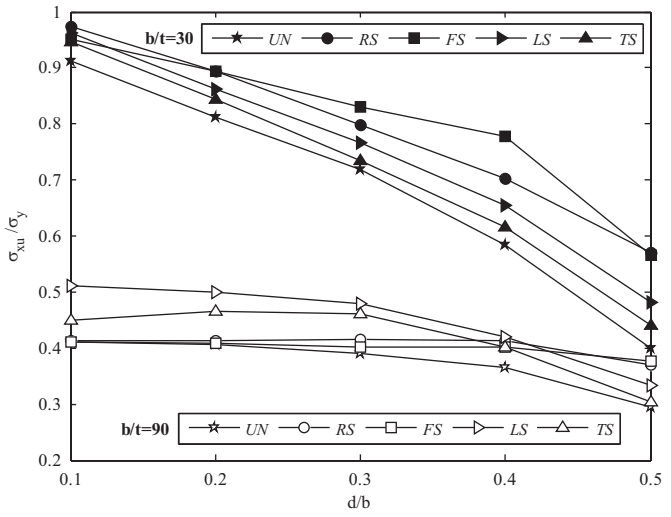

Fig. 7. Elasto-plastic ultimate strengths of unstrengthened and strengthened perforated plates with $b/t=30$ and 90.

ratios. The corresponding improvements in σ_{xu} of plates with $b/t=90$ are, respectively, 0–25%, 0–27%, 13–24% and 3–18%, and the values of *RS*-strengthened and *FS*-strengthened plates (or *LS*-strengthened and *TS*-strengthened plates) with large holes are obviously greater (or less) than those of plates with small holes. Hence, conclusion can be made from strength variation with hole size and comparison of stiffener types that *LS* and *TS* bring the best strengthening effects for thin plates (e.g., $b/t=90$) with small or moderate holes (e.g., $d/b<0.4$), while the highest increases in σ_{xu} occur in *RS*-strengthened and *FS*-strengthened plates whose slenderness ratios are small (e.g., $b/t=30$) or slenderness ratios and hole sizes are both large (e.g., $b/t=90$ and $d/b>0.4$).

2. When d/b keeps constant, σ_{xu} of all strengthened perforated plates decrease obviously with increase in b/t, which is similar to elastic buckling stress.
3. For the cases of invariable b/t, σ_{xu} of all strengthened perforated plates, except for the *TS*-strengthened plates with large slenderness ratios, are rapidly (for small b/t) or slowly (for large b/t) decreased as d/b is increased.

Fig. 8 shows the stress distributions in limit state of the uniaxially compressed perforated square plates with centric circular cutouts, for the cases of plate slenderness ratio $b/t=30$ and hole diameter ratios $d/b=0.1$, 0.3 and 0.5. The red areas represent the plastic zones where the equivalent stresses are the highest and equal to yield stress. It is evident that the plastic zones are successive and cover most parts of the plate when the hole diameter is relatively small, indicating the full usage of most materials of the plate. While for the cases of large holes, these plastic zones are separated and reduced due to the remarkable influence of cutout on stress distribution. This is the reason why σ_{xu} falls obviously with increasing d/b when b/t keeps constant, as shown in Fig. 7.

Comparing the limit state stress results of strengthened and unstrengthened perforated plates, summaries can also be made as follows:

1. For the *RS*-strengthened plate, σ_{xu} is enhanced primarily due to increase in area of plastic zones caused by the presence of ringed stiffener. Especially for small hole of $d/b=0.1$, the *RS*-strengthened plate gives the largest σ_{xu} since the whole plate except two small zones near the hole edge reaches yield status.
2. For the *FS*-strengthened plate, the expansion of plastic zones becomes invisible (even diminished for large d/b) due to the load-bearing participation of flat stiffener. The natural cause of ultimate strength growth for the strengthened plate lies in the

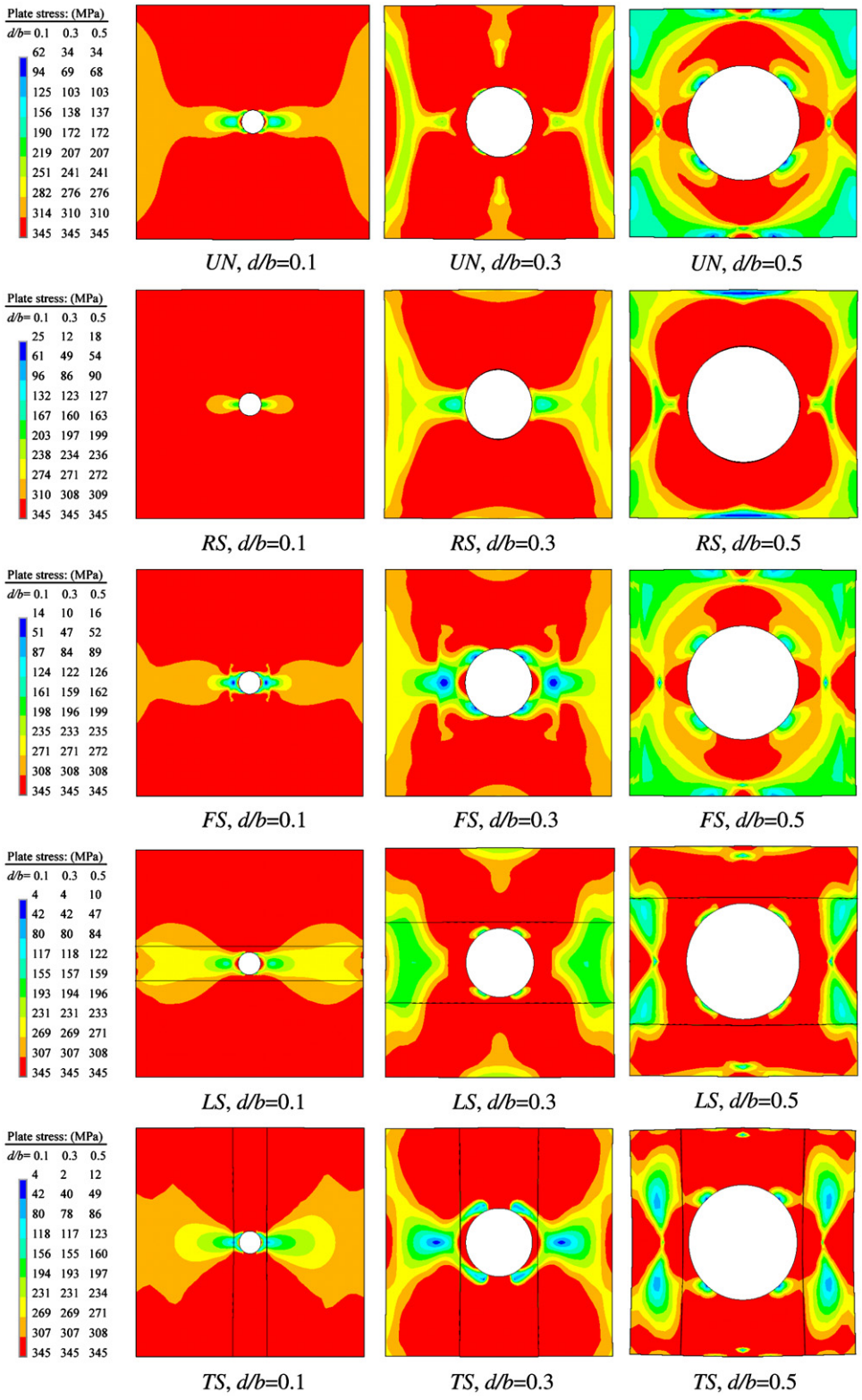

Fig. 8. Von Mises stress distributions in limit state for the perforated plates with $b/t=30$.

considerable contribution to the compression area provided by the large-ranged flat stiffener. The larger the d/b is, the more remarkable the contribution of flat stiffener.

3. For the *LS*-strengthened and *TS*-strengthened plates, limit state stress distributions are locally changed due to the existence of stiffeners and that variety becomes more obvious as d/b is increased. In the authors' opinion, the main causation of increases in σ_{xu} lies in the reduction of geometric nonlinear effect in large deformation state since the out-of-plane stiffnesses of the plates have been improved by the laterally placed stiffeners. It should also be noted that the influence of increase in compression area provided by the longitudinal

stiffeners, which are placed parallel to the load direction on the elasto-plastic buckling strengths of *LS*-strengthened plates should not be neglected.

4.3. Elastic buckling versus elasto-plastic buckling

As has been declared in published literatures, the elastic buckling critical stress of a relatively thick plate under in-plane compression is normally larger than the elasto-plastic ultimate strength even material yield stress, which leads to the so-called elasto-plastic buckling of plate. While for a thin plate whose slenderness ratio is relatively large, the situation is reversed and the ultimate strength is higher than the elastic buckling stress due to the post-buckling behavior of the plate. Fig. 9 shows the elastic and elasto-plastic buckling stresses of uniaxially compressed perforated square plates with centric circular holes, as plotted against the plate slenderness ratio. It is clear that σ_{cr} and σ_{xu} both rise when b/t decreases, while the slopes of two curves are rather different, i.e., the elevation in σ_{cr} due to the decrease of b/t is obviously faster than that in σ_{xu} for the same d/b. Hence, there is a turning point, as determined by the intersection of elastic and elasto-plastic curves, between the two buckling patterns for a perforated plate. The corresponding b/t of the turning point is defined as the critical slenderness ratio (i.e., $[b/t]_{cr}$), which has been used to identify the probable buckling/failure pattern of the plate. When $b/t < [b/t]_{cr}$, the out-of-plane deformations of the plate increase as the applied loads are increased and the failure eventually happens after the material has reached the yield point (or according to some yield criteria). While for the cases of $b/t > [b/t]_{cr}$, elastic buckling occurs prior to elasto-plastic buckling and the difference between σ_{cr} and σ_{xu} enlarges gradually as b/t is increased.

A similar situation appears in the strengthened perforated plates and the critical slenderness ratios of unstrengthened and strengthened perforated plates with varying hole diameter ratios are demonstrated in Fig. 10. For *FS*-strengthened and *LS*-strengthened plates, $[b/t]_{cr}$ for $d/b=0.1$–0.5 are restricted to a narrow value range whose bandwidth is no larger than 8, and the variations of critical slenderness ratio with hole size are similar to that of unstrengthened perforated plate, i.e., $[b/t]_{cr}$ first increases and then decreases as d/b is enlarged. But $[b/t]_{cr}$ of these two types of strengthened plates are decreased by 2–12% and increased by 50–75%, respectively, when compared to the unstrengthened

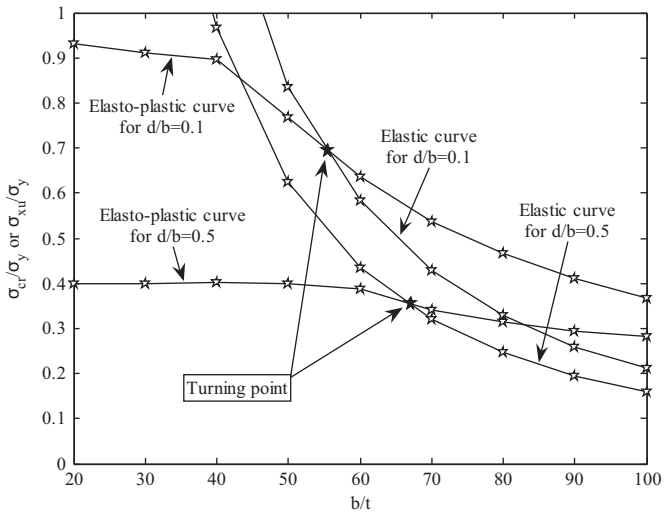

Fig. 9. Elastic and elasto-plastic buckling stresses of uniaxially compressed perforated square plates with centrally placed circular holes.

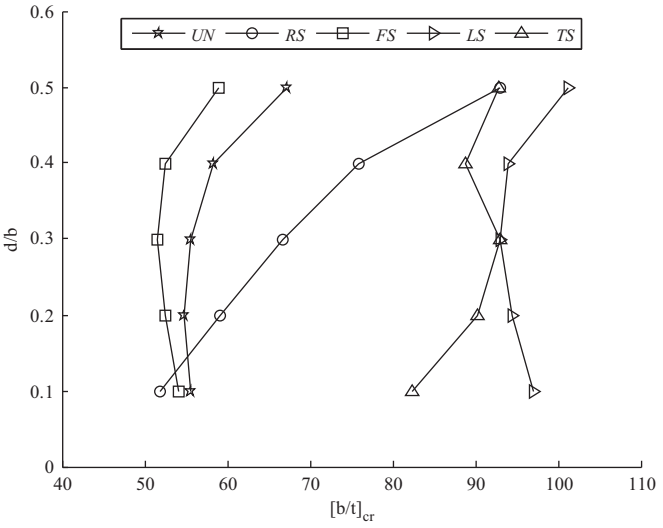

Fig. 10. Critical slenderness ratios of strengthened and unstrengthened perforated plates.

ones. As a trend, $[b/t]_{cr}$ of *RS*-strengthened plates becomes larger when d/b increases and covers a wide value range from 51 to 93 for $d/b=0.1$–0.5. $[b/t]_{cr}$ of *TS*-strengthened plates takes high values between 82 and 93, while the variations of $[b/t]_{cr}$ with d/b are ruleless due to buckling mode alteration.

5. Comparison of strengthening efficiency

The previous analyses are carried out on the basis of the selected geometric sizes of stiffeners as introduced earlier, implying that buckling behavior improving of strengthened plates are obtained at different costs of steel consumption which has been the concern of designers. In this regard, further comparisons of strengthening efficiency by investigating the variations of buckling stress with stiffener geometric size are carried out. In the following analyses, more cases of stiffener sizes are considered for a strengthened perforated plate with specific slenderness ratio and hole diameter ratio. The two types of buckling stresses, i.e., elastic buckling stress and elasto-plastic ultimate strength are, respectively, discussed.

5.1. Elastic buckling stress

Elastic buckling stress curves of four types of strengthened perforated plates with slenderness ratio $b/t=90$ and hole diameter ratio $d/b=0.3$ are simultaneously demonstrated in Fig. 11, as plotted against the relative stiffener weight, which is defined as the weight ratio of strengthening stiffener to strengthened plate. In the figure, strengthening efficiency can be easily estimated by curve location (i.e., the higher the curve locates, the more efficient the cutout-strengthening method is) or curve slope (i.e., the greater the gradient is, the more efficient the stiffener behaves). Obviously, *LS* and *TS* have the highest strengthening efficiencies since their curve slopes are much larger than those of other two types of stiffeners, while *FS* contributes nothing to the elastic behavior of the perforated plates within the considered scope of relative stiffener weight. Similar characteristics appear in all considered plates (i.e., the perforated plates with slenderness ratios $b/t=20$–100 and hole diameter ratios $d/b=0.1$–0.5). Hence, we conclude that *LS* and *TS* are the two most efficient stiffeners for improving the elastic behaviors of uniaxially compressed perforated square plates containing

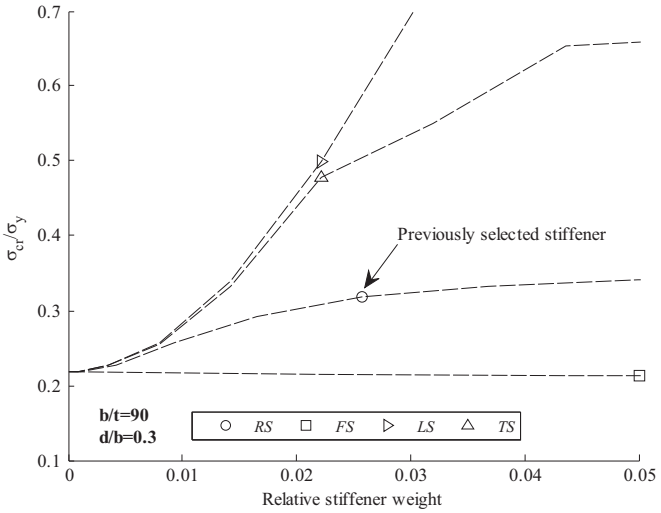

Fig. 11. Elastic buckling stress curves of the strengthened perforated plates with $b/t=90$ and $d/b=0.3$, as plotted against the relative stiffener weight.

centrally placed circular holes, with *LS* being especially suitable for the cases where the required increases in elastic buckling stress are relatively high.

5.2. Elasto-plastic ultimate strength

Fig. 12 shows the variations of ultimate strength with relative stiffener weight for the strengthened perforated plates with typical slenderness ratios and hole diameter ratios. The following are found:

5.2.1 *Cases of slenderness ratio* $b/t=30$: For the cases of $d/b=0.1$, *FS* and *RS* are the two most efficient stiffeners within the scope of relative stiffener weights considered in the research. However, the slope of *FS* curve gradually declines as the hole size is enlarged until its strengthening efficiency is overtaken by *RS* in the cases of $d/b=0.5$. The strengthening efficiencies of *LS* and *TS* are relatively insignificant, despite that the *LS*-curve is always located above the *TS*-curve for the same d/b.

5.2.2 *Cases of slenderness ratio* $b/t=60$: When $d/b=0.1$, *LS*-curve and *TS*-curve locate obviously higher than the other two curves, with *TS* being the most efficient for the cases of relatively small requirements in ultimate strength enhancement. For the cases of $d/b=0.3$, *LS*, *RS* and *TS* have similar strengthening efficiencies, which are much greater than *FS*. While for all types of strengthened plates with $d/b=0.5$, the ultimate strength of *RS*-strengthened plate is the highest when the relative stiffener weights are identical. On the whole, the competitive power of *RS* is gradually enhanced as d/b is increased, and the strengthening efficiencies provided by *FS* are as low as negligible when compared to the other stiffener types.

5.2.3 *Cases of slenderness ratio* $b/t=90$: *LS* always has the highest strengthening efficiency for all cases of hole diameter ratios (i.e., $d/b=0.1$–0.5). *RS* is more efficient for plates with large holes than for those of small hole diameter ratios, and *FS* has almost no contribution to the ultimate strength improvement, which is similar to the situations of relatively small slenderness ratios (e.g., $b/t=30$, 60).

It can be seen from the previous analyses that there is no one of the four types of stiffeners always behaves the highest

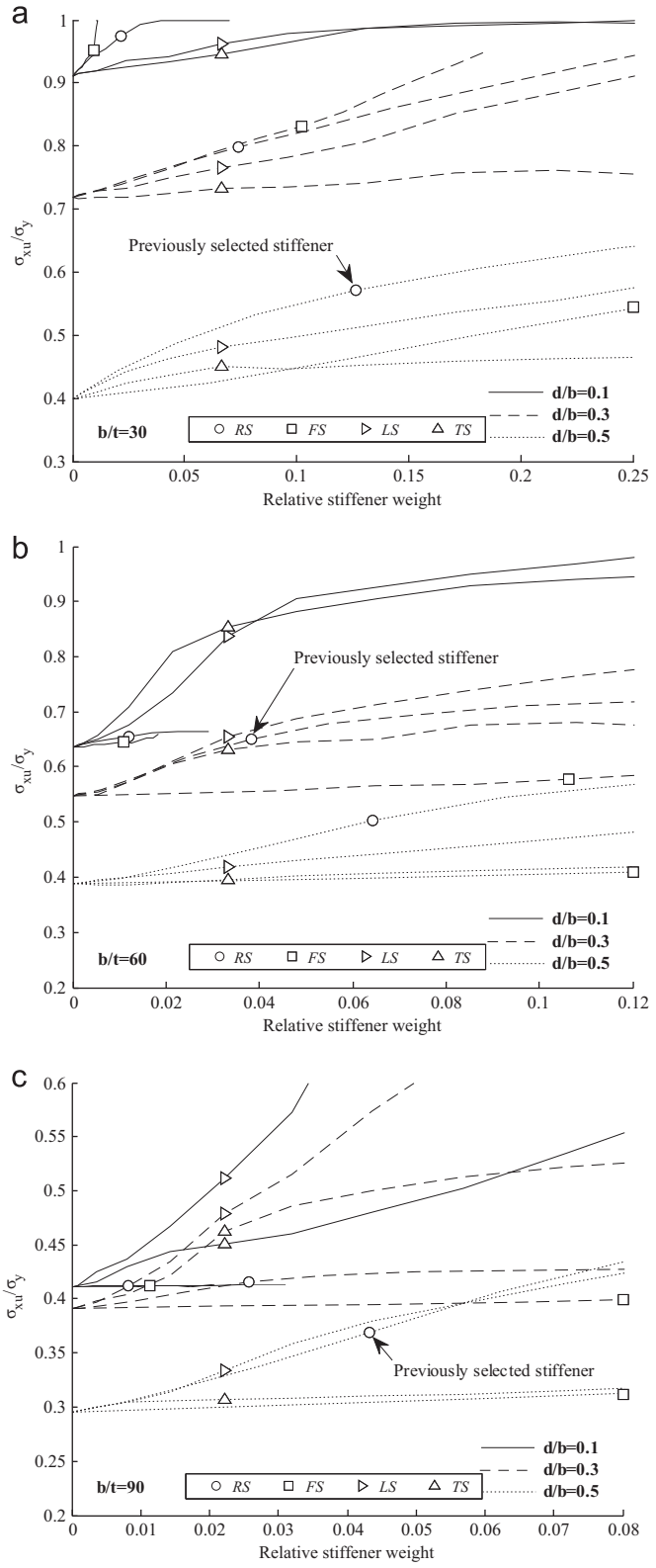

Fig. 12. Ultimate strength curves of the strengthened perforated plates, as plotted against the relative stiffener weight.

strengthening efficiency in ultimate strength enhancement for all perforated plates, which is rather different from the situations of elastic buckling. The most efficient stiffener, therefore, should be chosen according to geometric parameters of the perforated plate including plate slenderness ratios and hole diameter ratio. Based on the detailed comparative analyses on the strengthening

Table 1
Recommendations on the most efficient cutout-strengthening methods for improving the ultimate strengths of the uniaxially compressed perforated square plates with centric circular holes.

	Small holes	Medium-sized holes	Large holes
	($d/b \le 0.2$)	($0.2 < d/b < 0.4$)	($0.4 \le d/b \le 0.5$)
Thick plates ($b/t \le 40$)	*FS*	*FS* or *RS*	*RS*
Moderate thick plates ($40 < b/t < 80$)	*LS* or *TS*	*LS* or *TS* or *RS*	*RS*
Thin plates ($b/t \ge 80$)	*LS*	*LS*	*LS* or *RS*

efficiency of the perforated plates with typical slenderness ratios $b/t=30$, 60, 90 and typical hole diameter ratios $d/b=0.1$, 0.3, 0.5, recommendations on the most efficient cutout-strengthening methods for improving the ultimate strengths of the uniaxially compressed perforated square plates with centric circular holes are given in Table 1, in which the plates are divided into nine categories according to plate slenderness ratios (i.e., thick plates with $b/t \le 40$, moderately thick plates with $40 < b/t < 80$ and thin plate plates with $b/t \ge 80$) and hole diameter ratios (i.e., small holes with $d/b \le 0.2$, medium-sized holes with $0.2 < d/b < 0.4$ and large holes with $0.4 \le d/b \le 0.5$).

6. Conclusions

The present paper is dedicated to the buckling behaviors of uniaxially compressed perforated steel plates strengthened by four types of stiffeners, i.e., ringed stiffener, flat stiffener, longitudinal stiffener and transverse stiffener. Series of ANSYS elastic and elasto-plastic buckling finite element analyses were carried out with various plate slenderness ratios as well as circular hole diameter ratios.

It is found that the buckling behaviors of strengthened perforated plates are similar to those of unstrengthened ones. The elastic buckling stresses and elasto-plastic ultimate strengths of all strengthened perforated plates, when compared to the unstrengthened plates, are improved due to the presence of stiffeners discussed in the paper, while the increased amplitudes are greatly influenced by factors including stiffener type, plate slenderness ratio, hole diameter ratio, etc. In comparison, *RS* and *FS* give the best strengthening effects in elasto-plastic ultimate strengths for thick plates when stiffeners take the commonly used geometric sizes as mainly discussed in this paper, while the greatest increases in elasto-plastic ultimate strengths for thin plates and in elastic buckling stresses for all perforated plates are obtained from *LS*. Recommendations on the most efficient stiffeners for the strengthening of the uniaxially compressed perforated square plates with centrally placed circular holes are also proposed. These suggestions will be very useful for the selection of cutout-strengthening method in practical engineering.

Acknowledgement

The present research was undertaken with support from the Specialized Research Fund for the Doctoral Program of Higher Education Funded by the Ministry of Education of P.R.C. (no. 20090073120012).

References

[1] Shanmugam NE, Narayanan R. Elastic buckling of perforated square plates for various loading and edge conditions. In: Proceedings of the international conference on finite element methods, Shanghai, 1982.
[2] Sabir AB, Chow FY, Elastic buckling of flat panels containing circular and square holes. In: Proceedings of the international conference on instability and plastic collapse of steel structures, London, 1983. p. 311–21.
[3] Brown CJ, Yettram AL. The elastic stability of square perforated plates under combination of bending, shear and direct load. Thin-Walled Structures 1986;4:239–46.
[4] Brown CJ, Yettram AL, Burnett M. Stability of plates with rectangular holes. Journal of Structural Engineering—ASCE 1987;113:1111–6.
[5] Brown CJ. Elastic buckling of perforated plates subjected to concentrated loads. Computers and Structures 1990;36:1103–9.
[6] Shakerley TM, Brown CJ. Elastic buckling of plates with eccentrically positioned rectangular perforations. International Journal of Mechanical Sciences 1996;38:825–38.
[7] El-Sawy KM, Nazmy AS. Effect of aspect ratio on the elastic buckling of uniaxially loaded plates with eccentric holes. Thin-Walled Structures 2001;39:983–98.
[8] El-Sawy KM, Martini MI. Elastic stability of bi-axially loaded rectangular plates with a single circular hole. Thin-Walled Structures 2007;45:122–33.
[9] Moen CD, Schafer BW. Elastic buckling of thin plates with holes in compression or bending. Thin-Walled Structures 2009;47:1597–607.
[10] Narayanan R, Rockey KC. Ultimate load capacity of plate girders with webs containing circular cut-outs. Proceedings of the Institution of Civil Engineers 1981;71(2):845–62.
[11] Azizian ZG, Roberts TM. Buckling and elasto-plastic collapse of perforated plates. In: Proceedings of the international conference on instability and plastic collapse of steel structures, London, 1983. p. 392–8.
[12] Narayanan R, Chow FY. Ultimate capacity of uniaxially compressed perforated plates. Thin-Walled Structures 1984;2:241–64.
[13] Shanmugam NE, Thevendran V, Tan YH. Design formula for axially compressed perforated plates. Thin-Walled Structures 1999;34:1–20.
[14] El-Sawy KM, Nazmy AS, Martini MI. Elasto-plastic buckling of perforated plates under uniaxial compression. Thin-Walled Structures 2004;42:1083–101.
[15] Paik JK. Ultimate strength of perforated steel plates under edge shear loading. Thin-Walled Structures 2007;45:301–6.
[16] Paik JK. Ultimate strength of perforated steel plates under axial compressive loading along short edges. Ships and Offshore Structures 2007;2:3.
[17] Paik JK. Ultimate strength of perforated steel plates under combined biaxial compression and edge shear loads. Thin-Walled Structures 2008;46:207–13.
[18] Maiorana E, Pellegrino C, Modena C. Linear buckling analysis of perforated plates subjected to localized symmetrical load. Engineering Structures 2008;30:3151–8.
[19] Maiorana E, Pellegrino C, Modena C. Non-linear analysis of perforated steel plates subjected to localized symmetrical load. Journal of Constructional Steel Research 2009;65:959–64.
[20] ANSYS user's manual (version 10.0). Houston: Swanson Analysis System Inc.; 2005.